

---

# Learning Energy-Based Models by Cooperative Diffusion Recovery Likelihood

---

**Yaxuan Zhu**

Department of Statistics  
UCLA

**Jianwen Xie**

Akool Research

**Ying Nian Wu**

Department of Statistics  
UCLA

**Ruiqi Gao**

Google DeepMind

## Abstract

Training energy-based models (EBMs) with maximum likelihood estimation on high-dimensional data can be both challenging and time-consuming. As a result, there is a noticeable gap in sample quality between EBMs and other generative frameworks like GANs and diffusion models. To close this gap, inspired by the recent efforts of learning EBMs by maximizing diffusion recovery likelihood (DRL), we propose cooperative diffusion recovery likelihood (CDRL), an effective approach to tractably learn and sample from a series of EBMs defined on increasingly noisy versions of a dataset, paired with an initializer model for each EBM. At each noise level, the initializer model learns to amortize the sampling process of the EBM, and the two models are jointly estimated within a cooperative training framework. Samples from the initializer serve as starting points that are refined by a few sampling steps from the EBM. With the refined samples, the EBM is optimized by maximizing recovery likelihood, while the initializer is optimized by learning from the difference between the refined samples and the initial samples. We develop a new noise schedule and a variance reduction technique to further improve the sample quality. Combining these advances, we significantly boost the FID scores compared to existing EBM methods on CIFAR-10 and ImageNet 32x32, with a 2x speedup over DRL. In addition, we extend our method to compositional generation and image inpainting tasks, and showcase the compatibility of CDRL with classifier-free guidance for conditional generation, achieving similar trade-offs between sample quality and sample diversity as in diffusion models.

## 1 Introduction

Energy-based models (EBMs), as a class of probabilistic generative models, have exhibited their flexibility and practicality in a variety of application scenarios, such as realistic image synthesis [1, 2, 3, 4, 5, 6, 7, 8], graph generation [9], compositional generation [10, 11], video generation [12], 3D generation [13, 14, 15], simulation-based inference [16], stochastic optimization [17], out-of-distribution detection [18, 19], continue learning [20], internal learning [21], learning set function [22], image style transfer [23], continuous inverse optimal control [24], and latent space modeling [25]. Despite the recent successes of the EBMs, their training and sampling have been challenging because of the intractability of the normalizing constant.

Recently, the Diffusion Recovery Likelihood (DRL) [26] has emerged as a powerful framework for estimating EBMs. Inspired by diffusion models [27, 28, 29], DRL estimates a sequence of EBMs for the marginal distributions of a diffusion process, where each EBM is trained with recovery likelihood that maximizes the conditional probability of the data at the current noise level given their noisy versions at a higher noise level. Maximizing recovery likelihood is more tractable as sampling from the conditional distribution is much easier than sampling from the marginal distribution. DRL achieves exceptional generation performance among EBM-based generative models. However, a

noticeable performance gap still exists between the sample quality of EBMs and other generative frameworks like GANs or diffusion models. Moreover, DRL requires around 30 MCMC sampling steps at each noise level to generate valid samples, which can be time-consuming during both training and sampling processes.

To further close the performance gap and expedite EBM training and sampling with fewer MCMC steps, we introduce Cooperative Diffusion Recovery Likelihood (CDRL), that jointly estimates a sequence of EBMs and MCMC initializers defined on data perturbed by a diffusion process. At each noise level, the initializer and EBM are updated by cooperative training: The initializer model proposes initial samples by making prediction of the samples at the current noise level given their noisy versions at a higher noise level. The initial samples are then refined by a few MCMC sampling steps from the conditional distribution defined by the EBM. Given the refined samples, the EBM is updated by maximizing recovery likelihood, and the initializer is updated to absorb the difference between the initial samples and the refined samples. Compared to DRL, the introduced initializer models learn to accumulate the MCMC transitions of the EBMs and reproduces them by direct ancestral sampling, such that the MCMC sampling of the EBMs is amortized. Compared to [30] that applied cooperative training to an initializer and an EBM for the *marginal* distribution of the clean data, our approach only requires learning *conditional* initializers and sampling from *conditional* EBMs, which are much more tractable than their marginal counterparts. Combining with a new noise schedule and a variance reduction technique we develop, we achieve significantly better performance than existing methods of estimating EBMs. To boost the performance of conditional generation, we adapt class-free guidance (CFG) [31], a prominent technique for diffusion models, to our framework. We observe similar trade-offs between sample quality and sample diversity as CFG for diffusion models when adjusting the guidance strength. In addition, we showcase that our approach can be easily extended to perform compositional generation and image inpainting.

Our main contributions are as follows: (1) We propose cooperative diffusion recovery likelihood (CDRL) that tractably and efficiently learns and samples from a sequence of EBMs and MCMC initializers; (2) We propose a new noise schedule and a noise variance reduction technique that further improve the performance of CDRL; (3) Empirically We demonstrate that CDRL achieves significant improvements on sample quality compared to existing EBM approaches, on CIFAR-10 and ImageNet  $32 \times 32$  datasets; (4) We demonstrate CDRL’s ability in compositional generation, image inpainting, as well as its compatibility with classifier-free guidance for conditional generation.

## 2 Preliminaries on Energy-Based Models

Let  $\mathbf{x} \sim p_{\text{data}}(\mathbf{x})$  be a training example from an underlying data distribution. An energy-based model defines the density of  $\mathbf{x}$  by

$$p_{\theta}(\mathbf{x}) = \frac{1}{Z_{\theta}} \exp(f_{\theta}(\mathbf{x})), \quad (1)$$

where  $f_{\theta}$  is the unnormalized log density, or negative energy, parametrized by a neural network with a scalar output.  $Z_{\theta}$  is the normalizing constant or partition function. The derivative of the log-likelihood function of an EBM can be approximately written as

$$\mathcal{L}'(\theta) = \mathbb{E}_{p_{\text{data}}} \left[ \frac{\partial}{\partial \theta} f_{\theta}(\mathbf{x}) \right] - \mathbb{E}_{p_{\theta}} \left[ \frac{\partial}{\partial \theta} f_{\theta}(\mathbf{x}) \right], \quad (2)$$

where the second term is analytically intractable and has to be estimated by Monte Carlo samples from the current model  $p_{\theta}$ . Therefore, applying gradient-based optimization for an EBM usually involves an inner loop of MCMC sampling, which can be time-consuming for high-dimensional data.

## 3 Cooperative Diffusion Recovery Likelihood

### 3.1 Diffusion recovery likelihood

Following the design of Diffusion Recovery Likelihood (DRL) [26], we estimate a sequence of EBMs on increasingly noisy versions of data. Specifically, we assume a sequence of noise-perturbed training examples  $\mathbf{x}_0, \mathbf{x}_1, \dots, \mathbf{x}_T$  such that  $\mathbf{x}_0 \sim p_{\text{data}}$ ;  $\mathbf{x}_{t+1} = \alpha_{t+1}\mathbf{x}_t + \sigma_{t+1}\epsilon$ . In practice, a variance-preserving noise schedule [32] is applied so that  $\alpha_t = \sqrt{1 - \sigma_t^2}$ . We can also sample  $\mathbf{x}_t$  at an

arbitrary noise level directly from  $\mathbf{x}_0$  by  $\mathbf{x}_t = \bar{\alpha}_t \mathbf{x}_0 + \bar{\sigma}_t \epsilon$ , where  $\bar{\alpha}_t = \prod_{i=1}^t \alpha_i$  and  $\bar{\sigma}_t = \sqrt{1 - \bar{\alpha}_t}$ . Denote  $\mathbf{y}_t = \alpha_{t+1} \mathbf{x}_t$  for notation simplicity. The marginal distributions of  $\{\mathbf{y}_t; t = 1, \dots, T\}$  are modeled by a sequence of EBMs:  $p_\theta(\mathbf{y}_t) = \frac{1}{Z_{\theta,t}} \exp(f_\theta(\mathbf{y}_t; t))$ . Then the conditional EBM of  $\mathbf{y}_t$  given the sample at a higher noise level can be derived as

$$p_\theta(\mathbf{y}_t | \mathbf{x}_{t+1}) = \frac{1}{\tilde{Z}_\theta(\mathbf{x}_{t+1})} \exp\left(f_\theta(\mathbf{y}_t; t) - \frac{1}{2\sigma_{t+1}^2} \|\mathbf{y}_t - \mathbf{x}_{t+1}\|^2\right), \quad (3)$$

where  $\tilde{Z}_\theta(\mathbf{x}_{t+1})$  is the partition function of the conditional EBM dependent on  $\mathbf{x}_{t+1}$ . Comparing with the marginal EBM  $p_\theta(\mathbf{y}_t)$ , the extra quadratic term in  $p_\theta(\mathbf{y}_t | \mathbf{x}_{t+1})$  constrains the conditional energy landscape to be localized around  $\mathbf{y}_t$ , making the latter less multi-modal and therefore easier to sample from. In the extreme case when  $\sigma_{t+1}$  is infinitesimal,  $p_\theta(\mathbf{y}_t | \mathbf{x}_{t+1})$  is approximately a Gaussian distribution that can be tractably sampled from and has a close connection to diffusion models. See [26] for more details.

Since  $p_\theta(\mathbf{y}_t | \mathbf{x}_{t+1})$  is easier to sample from than  $p_\theta(\mathbf{y}_t)$ , we estimate model parameters  $\theta$  by maximizing the following recovery log-likelihood function at each noise level [33]:

$$\mathcal{J}_t(\theta) = \frac{1}{n} \sum_{i=1}^n \log p_\theta(\mathbf{y}_{t,i} | \mathbf{x}_{t+1,i}), \quad (4)$$

where  $\mathbf{y}_{t,i} \sim p_\theta(\mathbf{y}_t)$  and  $\mathbf{x}_{t+1,i}$  are the corresponding perturbed samples at noise level  $t+1$  for  $i = 1, \dots, n$ . Sampling from  $p_\theta(\mathbf{y}_t | \mathbf{x}_{t+1})$  can be achieved by running  $K$  steps of Langevin dynamics from some initialization point  $\tilde{\mathbf{y}}_t^0$  and iterating

$$\tilde{\mathbf{y}}_t^{\tau+1} = \tilde{\mathbf{y}}_t^\tau + \frac{s_t^2}{2} \left( \nabla_{\mathbf{y}} f_\theta(\tilde{\mathbf{y}}_t^\tau; t) + \frac{1}{\sigma_{t+1}^2} (\tilde{\mathbf{y}}_t^\tau - \mathbf{x}_{t+1}) \right) + s_t \epsilon^\tau \quad (5)$$

where  $s_t$  is the step size and  $\tau$  is the index of the current sampling step. DRL proposes to initialize the MCMC chain of noise level  $t$  using the sample  $\mathbf{x}_{t+1}$  from the higher noise level  $t+1$ . With the samples, the updating of EBMs then follows the same learning gradients as MLE (Equation 2), as the extra quadratic term  $-\frac{1}{2\sigma_{t+1}^2} \|\mathbf{y}_t - \mathbf{x}_{t+1}\|^2$  in  $p_\theta(\mathbf{y}_t | \mathbf{x}_{t+1})$  does not involve learnable parameters. DRL achieves strong generation quality with a sequence of 6 EBMs and 30 steps of Langevin dynamics for each noise level.

### 3.2 Amortizing MCMC sampling by initializer model

Although  $p_\theta(\mathbf{y}_t | \mathbf{x}_{t+1})$  is easier to sample from than  $p_\theta(\mathbf{y}_t)$ , when  $\sigma_{t+1}$  is not infinitesimal, the initialization of MCMC sampling,  $\mathbf{x}_{t+1}$ , may still be far from the data manifold of  $\mathbf{y}_t$ . This necessitates a certain amount of MCMC sampling steps at each noise level (e.g., 30 steps of Langevin dynamics in DRL). If the number of MCMC steps is insufficient or reduced, training may become unstable. This in turn limits the generation performance of DRL. Furthermore, as observed in [26], naively increasing the noise levels or the number of Langevin steps at each noise level does not significantly improve this problem. In fact, further increasing the Langevin steps from 30 to 50 only marginally influences the generation performance while greatly increasing training and sampling time.

To address this issue, we propose to learn an initializer model jointly with the EBM at each noise level, which maps  $\mathbf{x}_{t+1}$  closer to the manifold of  $\mathbf{y}_t$ . Specifically, the initializer model at noise level  $t$  is defined as

$$q_\phi(\mathbf{y}_t, t | \mathbf{x}_{t+1}) \sim \mathcal{N}(\mathbf{g}_\phi(\mathbf{x}_{t+1}; t), \tilde{\sigma}_t^2 \mathbf{I}). \quad (6)$$

It is a coarse approximation to  $p_\theta(\mathbf{y}_t | \mathbf{x}_{t+1})$ , as the former is a single-mode Gaussian distribution while the latter can be a multi-modal one. A more general formulation would be to involve latent variables  $\mathbf{z}_t$  following a certain simple prior  $p(\mathbf{z}_t)$  into  $\mathbf{g}_\phi$ . Then  $q_\phi(\mathbf{y}_t, t | \mathbf{x}_{t+1}) = \mathbb{E}_{p(\mathbf{z}_t)} [q_\phi(\mathbf{y}_t, \mathbf{z}_t, t | \mathbf{x}_{t+1})]$  can be non-Gaussian [34]. However, we empirically find that the simple initializer in Equation 6 works well. Comparing with the more general formulation, the simple initializer avoids the inference of  $\mathbf{z}_t$  which may again require MCMC sampling, and leads to more stable training. Different from [34], samples from the initializer just serves as the starting points and are refined by sampling from

the EBM, instead of being treated as the final samples. We follow [28] to set  $\tilde{\sigma}_t = \sqrt{\frac{1 - \bar{\alpha}_t^2}{1 - \bar{\alpha}_{t+1}^2}} \sigma_t$ . If we treat the sequence of initializers as the reverse process, such choice of  $\tilde{\sigma}_t$  corresponds to the lower bound of the standard deviation given by  $p_{\text{data}}$  being a delta function [27].

### 3.3 Cooperative training

We jointly train the sequence of EBMs and initializers in a cooperative fashion. Specifically, at each iteration for a randomly sampled noise level  $t$ , we obtain an initial sample  $\hat{\mathbf{y}}_t$  from the initializer model. Then a synthesized sample  $\tilde{\mathbf{y}}_t$  from  $p(\mathbf{y}_t|\mathbf{x}_{t+1})$  is generated by initializing from  $\hat{\mathbf{y}}_t$  and running a few steps of Langevin dynamics (Equation 5). The parameters of EBM are then updated by maximizing the recovery log-likelihood function (Equation 4). The learning gradient of EBM,  $\nabla_{\theta}\mathcal{J}_t(\theta)$ , is

$$\nabla_{\theta} \left[ \frac{1}{n} \sum_{i=1}^n f_{\theta}(\mathbf{y}_{t,i}; t) - \frac{1}{n} \sum_{i=1}^n f_{\theta}(\tilde{\mathbf{y}}_{t,i}; t) \right]. \quad (7)$$

To train the initializer model that amortizes the MCMC sampling process, we treat the revised sample  $\tilde{\mathbf{y}}_t$  by the EBM as the observed data of the initializer model, and estimate the parameters of the initializer by maximizing log-likelihood:

$$\mathcal{L}_t(\phi) = \frac{1}{n} \sum_{i=1}^n \left[ -\frac{1}{2\bar{\sigma}_t^2} \|\tilde{\mathbf{y}}_{t,i} - \mathbf{g}_{\phi}(\mathbf{x}_{t+1,i}; t)\|^2 \right]. \quad (8)$$

The initializer model learns to absorb the difference between  $\hat{\mathbf{y}}_t$  and  $\tilde{\mathbf{y}}_t$  at each iteration so that  $\hat{\mathbf{y}}_t$  is getting closer to the samples from  $p_{\theta}(\mathbf{y}_t|\mathbf{x}_{t+1})$ . In practice, we re-weight  $\mathcal{L}_t(\phi)$  across different noise levels by removing the coefficient  $\frac{1}{2\bar{\sigma}_t^2}$ , similar to the ‘‘simple loss’’ in diffusion models. The training algorithm is summarized in Algorithm 1.

After training, we generate new samples by starting from Gaussian white noise and progressively samples  $p_{\theta}(\mathbf{y}_t|\mathbf{x}_{t+1})$  at decreasingly lower noise levels. For each noise level, an initial proposal is generated from the initializer model, followed by a few steps of Langevin dynamics from the EBM. See Algorithm 2 for a summary.

### 3.4 Noise variance reduction

Besides introducing the initializer with cooperative training, we also propose a simple way to reduce the variance of learning EBMs by diffusion recovery likelihood. In the training of DRL, the pair of  $\mathbf{x}_t$  and  $\mathbf{x}_{t+1}$  is generated by  $\mathbf{x}_t \sim \mathcal{N}(\bar{\alpha}_t \mathbf{x}_0, \bar{\sigma}_t^2 \mathbf{I})$  and  $\mathbf{x}_{t+1} \sim \mathcal{N}(\alpha_{t+1} \mathbf{x}_t, \sigma_{t+1}^2 \mathbf{I})$ . Alternatively, we can fix the Gaussian white noise  $\mathbf{e} \sim \mathcal{N}(0, \mathbf{I})$ , and sample pair  $(\mathbf{x}'_t, \mathbf{x}'_{t+1})$  by

$$\begin{aligned} \mathbf{x}'_t &= \bar{\alpha}_t \mathbf{x}_0 + \bar{\sigma}_t \mathbf{e} \\ \mathbf{x}'_{t+1} &= \alpha_{t+1} \mathbf{x}'_t + \sigma_{t+1} \mathbf{e}. \end{aligned} \quad (9)$$

In other words, both  $\mathbf{x}'_t$  and  $\mathbf{x}'_{t+1}$  are linear interpolation between the clean sample  $\mathbf{x}_0$  and a given noise image  $\mathbf{e}$ .  $\mathbf{x}'_t$  and  $\mathbf{x}'_{t+1}$  have the same marginal distributions as  $\mathbf{x}_t$  and  $\mathbf{x}_{t+1}$ . But  $\mathbf{x}'_t$  is deterministic given  $\mathbf{x}_0$  and  $\mathbf{x}'_{t+1}$ , while there’s still variance for  $\mathbf{x}_t$  given  $\mathbf{x}_0$  and  $\mathbf{x}_{t+1}$ . The above scheme is related to the probability flow ODE for reversing the forward diffusion process [32].

### 3.5 Noise schedule and conditioning input

We improve upon the noise schedule and conditioning input of DRL. Let  $\lambda_t = \log \frac{\bar{\alpha}_t^2}{\bar{\sigma}_t^2}$  denote the logarithm of signal-to-noise ratio at noise level  $t$ . Inspired by [35], we send  $\lambda_t$  as the conditioning input to  $f_{\theta}$  and  $\mathbf{g}_{\phi}$  instead of  $t$ .

For the noise schedule, we keep the design of using 6 noise levels as in DRL. Inspired by [36], we construct a cosine schedule such that  $\lambda_t$  is defined as  $\lambda_t = -2 \log(\tan(at + b))$ .  $a$  and  $b$  are calculated from the maximum log SNR (denoted as  $\lambda_{\max}$ ) and minimum log SNR (denoted as  $\lambda_{\min}$ ) using:

$$b = \arctan(\exp(-0.5\lambda_{\max})), \quad a = \arctan(\exp(-0.5\lambda_{\min})) - b. \quad (10)$$

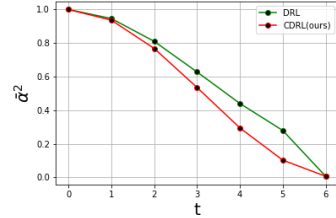


Figure 1: Noise level schedule. The green line is the noise levels used by DRL [26] while the red line is the noise levels used by our CDRL.

---

**Algorithm 1** CDRL Training

---

**Input:** (1) observed data  $\mathbf{x}_0 \sim p_{\text{data}}(\mathbf{x})$ ; (2) Number of noise level  $T$ ; (3) Number of Langevin sampling step  $K$  per noise level; (4) Langevin step size at each noise level  $s_t$ ; (5) Learning rate  $\eta_\theta$  for EBM  $f_\theta$ ; (6) Learning rate  $\eta_\phi$  for initializer  $g_\phi$ ;

**Output:** Parameters  $\theta, \phi$

Randomly initialize  $\theta$  and  $\phi$ .

**repeat**

  Sample noise level  $t$  from  $\{0, 1, \dots, T - 1\}$ .

  Sample  $\epsilon \sim \mathcal{N}(0, \mathbf{I})$ . Let  $\mathbf{x}_{t+1} = \bar{\alpha}_{t+1}\mathbf{x}_0 + \bar{\sigma}_{t+1}\epsilon$ ,  $\mathbf{y}_t = \alpha_{t+1}(\bar{\alpha}_t\mathbf{x}_0 + \bar{\sigma}_t\epsilon)$ .

  Generate the initial sample  $\hat{\mathbf{y}}_t$  following Equation 6.

  Generate the refined sample  $\mathbf{y}_t$  by running  $K$  steps of Langevin dynamics starting from  $\hat{\mathbf{y}}_t$  following Equation 5.

  Update EBM parameter  $\theta$  following the gradients in Equation 7.

  Update initializer parameter  $\phi$  by maximizing Equation 8.

**until** converged

---



---

**Algorithm 2** CDRL Sampling

---

**Input:** (1) Number of noise level  $T$ ; (2) Number of Langevin sampling step  $L$  at each noise level; (3) Langevin step size at each noise level  $\delta_t$ ; (4) Trained EBM  $f_\theta$ ; (5) Trained initializer  $g_\phi$ ;

**Output:** Samples  $\tilde{\mathbf{x}}_0$

Randomly initialize  $\mathbf{x}_T \sim \mathcal{N}(0, \mathbf{I})$ .

**for**  $t = T - 1$  **to** 0 **do**

  Generate initial proposal  $\hat{\mathbf{y}}_t$  following Equation 6.

  Update  $\hat{\mathbf{y}}_t$  to  $\tilde{\mathbf{y}}_t$  by  $K$  iterations of Equation 5.

  Let  $\tilde{\mathbf{x}}_t = \tilde{\mathbf{y}}_t / \alpha_{t+1}$ .

**end for**

---

We set  $\lambda_{\max} = 9.8$  and  $\lambda_{\min} = -5.1$  to match the accumulative noise level  $\bar{\alpha}_t$  of the original Recovery Likelihood model T6 at the highest and lowest noise levels. Figure 1 illustrates the noise schedule of DRL and our proposed schedule. Compared to DRL’s original schedule, our new schedule focuses more on regions with lower signal-to-noise ratios, crucial for generating low-frequency, high-level concepts in samples.

### 3.6 Conditional sampling and classifier-free guidance of energy-based models

[31] proposed classifier-free guidance that greatly improves the sample quality of conditional diffusion models, and trades-off between sample quality and sample diversity by adjusting the guidance strength. Given the close connection between EBMs and diffusion models, we show that it is possible to apply classifier-free guidance in CDRL as well. Specifically, suppose  $c$  is the context (e.g., a label or a text description). At each noise level we jointly estimate an unconditional EBM  $p_\theta(\mathbf{y}_t) \propto \exp(f_\theta(\mathbf{y}_t; t))$  and a conditional EBM  $p_\theta(\mathbf{y}_t|c) \propto \exp(f_\theta(\mathbf{y}_t; c, t))$ . By Bayes rule we have:

$$p_\theta(c|\mathbf{y}_t) = \frac{p_\theta(c, \mathbf{y}_t)}{p_\theta(\mathbf{y}_t)} = \frac{p_\theta(\mathbf{y}_t|c)p(c)}{p_\theta(\mathbf{y}_t)}. \quad (11)$$

With classifier-free guidance in sampling, we assume the log-density of  $\mathbf{y}_t$  is modified to

$$\log \tilde{p}(\mathbf{y}_t|c) = \log [p(\mathbf{y}_t|c)p(c|\mathbf{y}_t)^w] + \text{const} = (w + 1)f_\theta(\mathbf{y}_t; c, t) - wf_\theta(\mathbf{y}_t; t) + \text{const.}, \quad (12)$$

where  $w$  controls the guidance strength. When running Langevin sampling from the conditional EBM (Equation 5),  $f_\theta$  is revised to  $\tilde{f}_\theta(\mathbf{y}; c, t) = (w + 1)f_\theta(\mathbf{y}_t; c, t) - wf_\theta(\mathbf{y}_t; t)$ . Similarly, for the initializer model, we jointly estimate an unconditional model  $q_\phi(\mathbf{y}_t, t|\mathbf{x}_{t+1}) \sim \mathcal{N}(\mathbf{g}_\phi(\mathbf{x}_{t+1}; t), \tilde{\sigma}_t^2 \mathbf{I})$  and a conditional model  $q_\phi(\mathbf{y}_t, t|c, \mathbf{x}_{t+1}) \sim \mathcal{N}(\mathbf{g}_\phi(\mathbf{x}_{t+1}; c, t), \tilde{\sigma}_t^2 \mathbf{I})$ . Since both models follow Gaussian distribution, according to [37] the modified conditional model with classifier(-free) guidance is still a Gaussian, with the sample mean updated to  $(w + 1)\mathbf{g}_\phi(\mathbf{x}_{t+1}; c, t) - w\mathbf{g}_\phi(\mathbf{x}_{t+1}; t)$  and the variance remains the same.

In practice, we follow [31] to let the conditional and unconditional models share the same network both the EBM and the initializer model. The unconditional model is trained by setting an “empty”

class label  $c = \emptyset$ . During training, we randomly mask the label information with a probability  $p$  and jointly train the conditional and unconditional models.

### 3.7 Compositionality in energy-based model

One attractive property of EBMs is compositionality: one can combine the EBMs of separate independent random variables to compose a new joint EBM. Given two EBMs  $p_\theta(\mathbf{x}|c_1) \propto \exp(f_\theta(\mathbf{x}; c_1))$  and  $p_\theta(\mathbf{x}|c_2) \propto \exp(f_\theta(\mathbf{x}; c_2))$  that are conditional on two separate concepts, [10, 7, 11] constructs a new EBM conditional on both concepts as  $p_\theta(\mathbf{x}|c_1, c_2) \propto \exp(f_\theta(\mathbf{x}; c_1) + f_\theta(\mathbf{x}; c_2))$  based on the production of expert [38]. Here we show that a negative energy term is missing in that formulation, which can be easily added back with classifier-free guidance and leads to better compositional generation empirically. Specifically, suppose the two concepts  $c_1$  and  $c_2$  are conditionally independent given the observed data  $\mathbf{x}$ . Then we have

$$\begin{aligned} \log p_\theta(\mathbf{x}|c_1, c_2) &= \log p_\theta(\mathbf{x}, c_1, c_2) - \log p(c_1, c_2) = \log p_\theta(c_1, c_2|\mathbf{x}) + \log p_\theta(\mathbf{x}) - \log p(c_1, c_2) \\ &= \log p_\theta(c_1|\mathbf{x}) + \log p_\theta(c_2|\mathbf{x}) + \log p_\theta(\mathbf{x}) - \log p(c_1, c_2) \\ &= \log p_\theta(\mathbf{x}|c_1) + \log p_\theta(\mathbf{x}|c_2) - \log p_\theta(\mathbf{x}) - \log p(c_1, c_2) + \log p(c_1) + \log p(c_2) \\ &= f_\theta(\mathbf{x}; c_1, t) + f_\theta(\mathbf{x}; c_2, t) - f_\theta(\mathbf{x}; t) + \text{const.} \end{aligned} \quad (13)$$

Our formulation is similar to [11] and different from the one used in [10, 7] in the sense that an additional term  $-f_\theta(\mathbf{x}; t)$  is included to the unnormalized log-density, which can be easily derived from the joint training of the conditional and unconditional models in classifier-free guidance.

The composition can be generalized to include arbitrary number of concepts. Suppose we have  $M$  conditionally independent concepts  $c_i, i = 1, \dots, M$ , then

$$\log p_\theta(\mathbf{x}|c_i, i = 1, \dots, M) = \sum_{i=1}^M f_\theta(\mathbf{x}; c_i, t) - (M - 1)f_\theta(\mathbf{x}; t) + \text{const.} \quad (14)$$

We can combine the compositional log-density (Equation 14) with classifier-free guidance (Equation 12) to further improve the alignment of generated samples with given concepts. The log-density function is given by

$$\begin{aligned} &\log [p(\mathbf{x}|c_i, i = 1, \dots, M)p(c_i, i = 1, \dots, M|\mathbf{x})^w] \\ &= (w + 1) \sum_{i=1}^M f_\theta(\mathbf{x}; c_i, t) - (Mw + M - 1)f_\theta(\mathbf{x}; t) + \text{const.} \end{aligned} \quad (15)$$

To demonstrate the effectiveness of compositionality, we apply the formulation of compositional EBM to every noise level, and use simple unconditional initializer models.

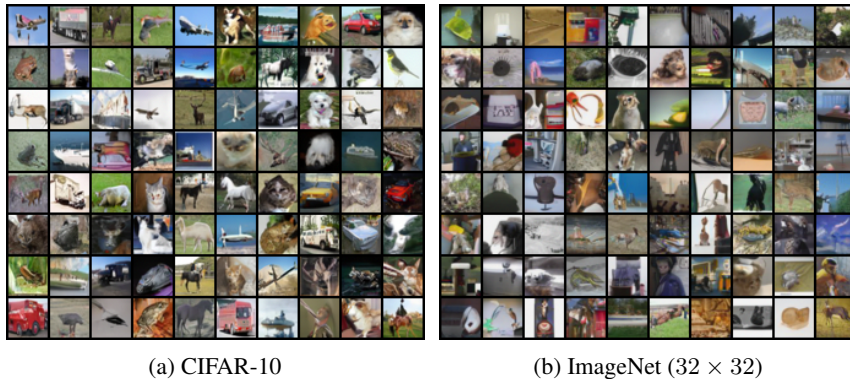


Figure 2: Unconditional generated examples on CIFAR-10 and ImageNet (32 × 32) datasets.

## 4 Experiments

We assess our model’s performance in different scenarios. Section 4.1 covers unconditional generation, Section 4.2 focuses on conditional generation and classifier-free guidance results, and Sections 4.3

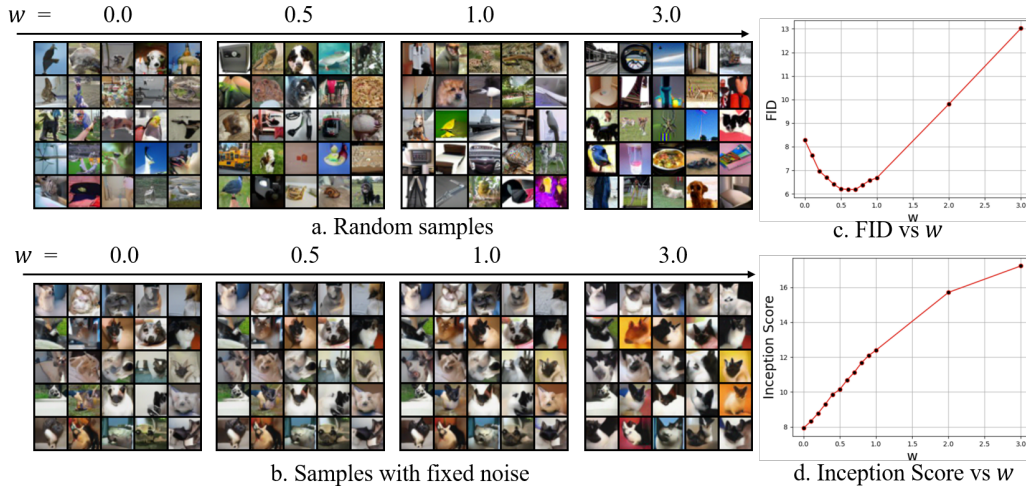


Figure 3: Conditional generation on ImageNet ( $32 \times 32$ ) with classifier free guidance. (a) Random samples generated under different guided weights  $w$ ; (b) Samples generated with fixed noise under different guided weights. The class label is set to be Siamese Cat. Sub-images at the same position are samples with the same random noise as well as class label and only differ in the guided weight; (c) FID Scores at different guided weight  $w$ ; (d) Inception Scores at different guided weight  $w$ .

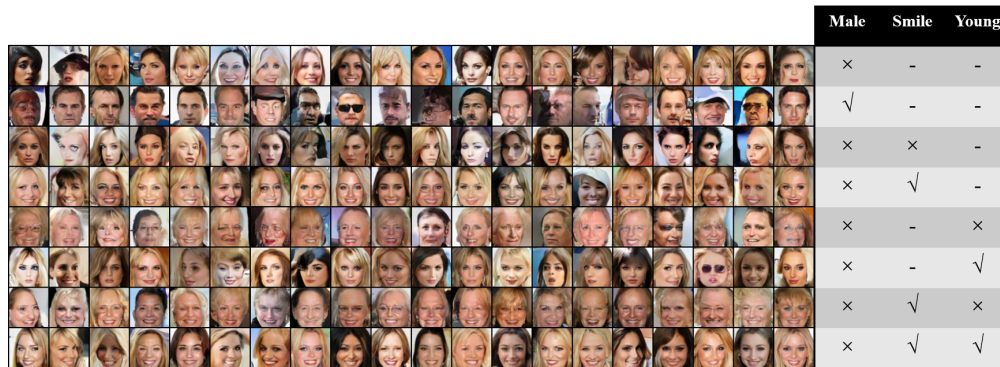


Figure 4: Attribute-compositional generation on CelebA ( $64 \times 64$ ) with guided weight  $w = 3$ . Left: generated samples under different attribute compositions. Right: control attributes ('√', '×' and '-' indicate true, false and no control respectively).

and 4.4 showcase our model’s compositionality and image inpainting abilities. We include training details and additional experiments for ablation studies in the Supplementary Material.

Our evaluations primarily involve three datasets: (i) CIFAR-10 [39] comprises images from 10 categories, with 50k training samples and 10k test samples at a resolution of  $32 \times 32$ . We use its training set for unconditional generation. (ii) ImageNet [40] contains approximately 1.28M images from 1000 categories. We use its training set for both conditional and unconditional generation, focusing on a downsampled version ( $32 \times 32$ ) of the dataset. (iii) CelebA [41] consists of around 200k human face images, each annotated with attributes. We downsample the dataset to  $64 \times 64$  and use it for compositionality and image inpainting tasks.

#### 4.1 Unconditional image generation

We first showcase our model’s capabilities in unconditional generation tasks. FID scores [42] are reported in Tables 1 and 2, with generated examples displayed in Figure 2. Our model, referred to as CDRL, uses the same EBMs structure as DRL [26]. We also employ a larger version called CDRL-large, featuring twice as many channels in each layer. Compared to DRL in [26], our CDRL achieves significant improvements in FID scores. Additionally, CDRL uses the same number of noise levels (6 in total) as DRL but requires only half the MCMC steps at each noise level (reduced from 30

Table 1: FID for CIFAR-10 unconditional generation.

Models	FID ↓	Models	FID ↓
EBM based method		Other likelihood based method	
NT-EBM [43]	78.12	VAE [51]	78.41
LP-EBM [25]	70.15	PixelCNN [52]	65.93
Adaptive CE [44]	65.01	PixelIQN [53]	49.46
EBM-SR [2]	44.50	Residual Flow [54]	47.37
JEM [18]	38.40	Glow [55]	45.99
EBM-IG [3]	38.20	DC-VAE [56]	17.90
EBM-FCE [45]	37.30	GAN based method	
CoopVAEBM [46]	36.20	WGAN-GP[57]	36.40
CoopNets [47]	33.61	SN-GAN [58]	21.70
Divergence Triangle [48]	30.10	BigGAN [59]	14.80
VARA [8]	27.50	StyleGAN2-DiffAugment [60]	5.79
EBM-CD [49]	25.10	Diffusion-GAN [34]	3.75
GEBM [4]	19.31	StyleGAN2-ADA [61]	2.92
HAT-EBM [5]	19.30	Score based and Diffusion method	
CF-EBM [23]	16.71	NCSN [29]	25.32
CoopFlow [50]	15.80	NCSN-v2 [62]	10.87
CLEL-base [7]	15.27	NCSN++ [32]	2.20
VAEBM [6]	12.16	DDPM Distillation [63]	9.36
DRL [26]	9.58	DDPM++(VP, NLL) [64]	3.45
CLEL-large [7]	8.61	DDPM [28]	3.17
CDRL (Ours)	4.31	DDPM++(VP, FID) [64]	2.47
CDRL-large (Ours)	3.68		

to 15), significantly lowering computational costs. Currently, CDRL reaches the state-of-the-art EBM framework, and its best results are comparable to strong baselines from other generative frameworks.

## 4.2 Conditional synthesis with classifier-free guidance

We evaluate our model for conditional generation on the ImageNet32 dataset, employing classifier-free guidance as outlined in Section 3.6. Generation results for varying guided weights  $w$  are displayed in Figure 3. As  $w$  increases, sample quality improves, and the conditioned class features become more prominent, though diversity may decrease. This is also evident from the FID and Inception Score [65] curves in Figures 3c and 3d. While the Inception Score consistently improves (increasing), the FID score first improves (decreasing) and then worsens (increasing), reaching the optimal value of 6.18 at a guidance weight of 0.7. Additional generation results can be found in the Supplementary Material.

Table 2: FID for ImageNet ( $32 \times 32$ ) unconditional generation.

Models	FID ↓
EBM-IG [3]	60.23
PixelCNN [52]	40.51
EBM-CD [49]	32.48
CF-EBM [23]	26.31
CLEL-base [7]	22.16
DRL [26]	- (not converge)
DDPM++(VP, NLL) [64]	8.42
CDRL (Ours)	9.35

## 4.3 Compositionality

We conduct experiments on CelebA ( $64 \times 64$ ) datasets, following Equation 15, with *Male*, *Smile*, and *Young* as controlled attributes. Similar to conditional sampling, we allow  $f_{\theta_i}(\mathbf{y}_t, c_i, t)$  to share the same network and learn the unconditional model with  $c = \emptyset$ . Specifically, we treat images with a certain attribute value as individual classes. We randomly assign each image in a training batch to a class based on the controlled attribute value. For example, an image with Male=True and Smile=True may be assigned to class 0 if the Male attribute is picked or class 2 if the Smile attribute is picked. For the conditional network structure, we make EBM  $f_{\theta}$  conditional on attributes  $c_i$  and use an unconditional initializer model  $g_{\phi}$  to propose the initial distribution. We focus on showcasing the

compositionality ability of EBM itself, although it is also possible to use a conditional initializer model similar to Section 3.6. Our results are displayed in Figure 4, with images generated at a guided weight of  $w = 3.0$ . More generation results with different guidance weights can be found in Figure in the Supplementary Material. Images generated with composed attributes following Equation 15 contain features of both attributes, and increasing the guided weight makes the corresponding attribute more prominent. This demonstrates CDRL’s ability and the effectiveness of Equation 15.

#### 4.4 Image inpainting

We demonstrate our learned model’s inpainting ability on the  $64 \times 64$  CelebA dataset. For each image, we mask a portion and let the model fill in the masked area. We add noise to the masked image up to the final noise level and allow the model to gradually denoise the image, similar to the standard generation process. During inpainting, we only update the masked area, retaining the unmasked area’s values. This is achieved by resetting the unmasked area values to the current noisy version after each Langevin update step of the EBM or initializer proposal step. Our results are shown in Figure 5. We test two masking types: a regular square mask and an irregularly shaped mask. CDRL successfully inpaints valid and diverse values in the masked area, with inpainted results differing from the observations. This indicates that our model does not merely memorize data points but fills in meaningful unobserved areas based on the dataset’s statistical features.

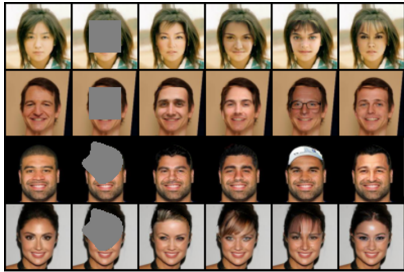


Figure 5: Image inpainting results on CelebA ( $64 \times 64$ ). The first two rows use square masks and the last two rows uses irregular masks. Column one displays original images. Column two shows masked images. Columns three to six exhibit inpainted images using different initialization seeds.

### 5 Related Work

**Energy-Based Learning** Energy-based models (EBMs) [66, 67, 68, 69] define unnormalized probabilistic distributions and are typically trained through maximum likelihood estimation. Methods such as contrastive divergence [38, 49], persistent chain [1], replay buffer [3] or short-run MCMC sampling [2] approximate the analytically intractable learning gradient. To scale up and stabilize EBM training for high-fidelity data generation, strategies like multi-grid sampling [70], progressive training [23], and diffusion [26] have been adopted. EBMs have also been connected to other models, such as adversarial training [4, 71], variational autoencoders [6], contrastive guidance [7], and noise contrastive estimation [45]. To alleviate MCMC burden, various methods have been proposed, including amortizing MCMC sampling with learned networks [72, 47, 73, 6, 74, 75]. Among them, cooperative networks (CoopNets) [47] jointly train a top-down generator and an EBM via MCMC teaching, using the generator as a fast initializer for Langevin sampling. CoopNets variants have also been studied [46, 50]. Our work improves the recovery likelihood learning algorithm of EBMs [26] by learning a fast MCMC initializer for EBM sampling, leveraging the cooperative learning scheme.

**Diffusion Model** Our work connects to diffusion models [28, 34] by learning a sequence of EBMs and MCMC initializers to reverse the diffusion process. Contrasting [28], our framework employs more expressive conditional EBMs instead of normal distributions. [34] also suggests multimodal distributions, trained by generative adversarial networks [76], for the reverse process.

### 6 Conclusion and Future Work

We propose CDRL, an EBM learning method employing cooperative diffusion recovery likelihood, significantly improving generation performance of EBMs. CDRL excels in compositional generation, image inpainting, and compatibility with classifier-free guidance for conditional generation. The present limitation might be the fact that a certain number of MCMC steps is still needed during generation. Besides, we also seek to scale our model for high-resolution image generation in the future. Our work aims to promote further research on EBMs as generative models. However, powerful generative models may pose negative social impacts, such as deepfakes, misinformation, privacy invasion, and eroding public trust, necessitating exploration of effective preventive measures.

## References

- [1] Jianwen Xie, Yang Lu, Song-Chun Zhu, and Ying Nian Wu. A theory of generative convnet. In *Proceedings of the 33rd International Conference on Machine Learning, ICML*, 2016.
- [2] Erik Nijkamp, Mitch Hill, Song-Chun Zhu, and Ying Nian Wu. Learning non-convergent non-persistent short-run MCMC toward energy-based model. In *Advances in Neural Information Processing Systems*, 2019.
- [3] Yilun Du and Igor Mordatch. Implicit generation and generalization in energy-based models. *arXiv preprint arXiv:1903.08689*, 2019.
- [4] Michael Arbel, Liang Zhou, and Arthur Gretton. Generalized energy based models. In *The Ninth International Conference on Learning Representations, ICLR*, 2021.
- [5] Mitch Hill, Erik Nijkamp, Jonathan Mitchell, Bo Pang, and Song-Chun Zhu. Learning probabilistic models from generator latent spaces with hat ebm. In *NeurIPS*, 2022.
- [6] Zhisheng Xiao, Karsten Kreis, Jan Kautz, and Arash Vahdat. Vaebm: A symbiosis between variational autoencoders and energy-based models. In *The Ninth International Conference on Learning Representations, ICLR*, 2021.
- [7] Hankook Lee, Jongheon Jeong, Sejun Park, and Jinwoo Shin. Guiding energy-based models via contrastive latent variables. In *The Eleventh International Conference on Learning Representations, ICLR*, 2023.
- [8] Will Sussman Grathwohl, Jacob Jin Kelly, Milad Hashemi, Mohammad Norouzi, Kevin Swersky, and David Duvenaud. No MCMC for me: Amortized sampling for fast and stable training of energy-based models. In *The Ninth International Conference on Learning Representations, ICLR*, 2021.
- [9] Meng Liu, Keqiang Yan, Bora Oztekin, and Shuiwang Ji. Graphebm: Molecular graph generation with energy-based models. In *EBM Workshop at ICLR*, 2021.
- [10] Yilun Du, Shuang Li, and Igor Mordatch. Compositional visual generation with energy based models. *Advances in Neural Information Processing Systems*, 2020.
- [11] Yilun Du, Conor Durkan, Robin Strudel, Joshua B Tenenbaum, Sander Dieleman, Rob Fergus, Jascha Sohl-Dickstein, Arnaud Doucet, and Will Grathwohl. Reduce, reuse, recycle: Compositional generation with energy-based diffusion models and mcmc. In *Proceedings of the Fortieth International Conference on Machine Learning, ICML*, 2023.
- [12] Jianwen Xie, Song-Chun Zhu, and Ying Nian Wu. Learning energy-based spatial-temporal generative convnets for dynamic patterns. *IEEE Transactions on Pattern Analysis and Machine Intelligence*, 43(2):516–531, 2021.
- [13] Jianwen Xie, Yifei Xu, Zilong Zheng, Song-Chun Zhu, and Ying Nian Wu. Generative pointnet: Deep energy-based learning on unordered point sets for 3d generation, reconstruction and classification. In *IEEE Conference on Computer Vision and Pattern Recognition, CVPR*, 2021.
- [14] Jianwen Xie, Zilong Zheng, Ruiqi Gao, Wenguan Wang, Song-Chun Zhu, and Ying Nian Wu. Learning descriptor networks for 3d shape synthesis and analysis. In *IEEE Conference on Computer Vision and Pattern Recognition, CVPR*, 2018.
- [15] Yaxuan Zhu, Jianwen Xie, and Ping Li. Likelihood-based generative radiance field with latent space energy-based model for 3d-aware disentangled image representation. In *International Conference on Artificial Intelligence and Statistics, AISTATS*, 2023.
- [16] Pierre Glaser, Michael Arbel, Arnaud Doucet, and Arthur Gretton. Maximum likelihood learning of energy-based models for simulation-based inference. *arXiv preprint arXiv:2210.14756*, 2022.
- [17] Lingkai Kong, Jiaming Cui, Yuchen Zhuang, Rui Feng, B. Aditya Prakash, and Chao Zhang. End-to-end stochastic optimization with energy-based model. In *NeurIPS*, 2022.
- [18] Will Grathwohl, Kuan-Chieh Wang, Jörn-Henrik Jacobsen, David Duvenaud, Mohammad Norouzi, and Kevin Swersky. Your classifier is secretly an energy based model and you should treat it like one. In *The Eighth International Conference on Learning Representations, ICLR*, 2020.
- [19] Weitang Liu, Xiaoyun Wang, John D. Owens, and Yixuan Li. Energy-based out-of-distribution detection. In *Advances in Neural Information Processing Systems*, 2020.

- [20] Fu-Yun Wang, Da-Wei Zhou, Liu Liu, Han-Jia Ye, Yatao Bian, De-Chuan Zhan, and Peilin Zhao. Beef: Bi-compatible class-incremental learning via energy-based expansion and fusion. In *The Eleventh International Conference on Learning Representations, ICLR, 2023*.
- [21] Zilong Zheng, Jianwen Xie, and Ping Li. Patchwise generative convnet: Training energy-based models from a single natural image for internal learning. In *IEEE Conference on Computer Vision and Pattern Recognition, CVPR*, pages 2961–2970, 2021.
- [22] Zijing Ou, Tingyang Xu, Qinliang Su, Yingzhen Li, Peilin Zhao, and Yatao Bian. Learning neural set functions under the optimal subset oracle. *NeurIPS*, 2022.
- [23] Yang Zhao, Jianwen Xie, and Ping Li. Learning energy-based generative models via coarse-to-fine expanding and sampling. In *The Ninth International Conference on Learning Representations, ICLR, 2021*.
- [24] Yifei Xu, Jianwen Xie, Tianyang Zhao, Chris Baker, Yibiao Zhao, and Ying Nian Wu. Energy-based continuous inverse optimal control. *IEEE Transactions on Neural Networks and Learning Systems*, 2022.
- [25] Bo Pang, Tian Han, Erik Nijkamp, Song-Chun Zhu, and Ying Nian Wu. Learning latent space energy-based prior model. In *Advances in Neural Information Processing Systems*, 2020.
- [26] Ruiqi Gao, Yang Song, Ben Poole, Ying Nian Wu, and Diederik P. Kingma. Learning energy-based models by diffusion recovery likelihood. In *The Ninth International Conference on Learning Representations, ICLR, 2021*.
- [27] Jascha Sohl-Dickstein, Eric A. Weiss, Niru Maheswaranathan, and Surya Ganguli. Deep unsupervised learning using nonequilibrium thermodynamics. In *Proceedings of the 32nd International Conference on Machine Learning, ICML, 2015*.
- [28] Jonathan Ho, Ajay Jain, and Pieter Abbeel. Denoising diffusion probabilistic models. In *Advances in Neural Information Processing Systems*, 2020.
- [29] Yang Song and Stefano Ermon. Generative modeling by estimating gradients of the data distribution. In *Advances in Neural Information Processing Systems*, 2019.
- [30] Jianwen Xie, Yang Lu, Ruiqi Gao, Song-Chun Zhu, and Ying Nian Wu. Cooperative training of descriptor and generator networks. *IEEE Trans. Pattern Anal. Mach. Intell.*, 42(1):27–45, 2020.
- [31] Jonathan Ho and Tim Salimans. Classifier-free diffusion guidance. *arXiv preprint arXiv:2207.12598*, 2022.
- [32] Yang Song, Jascha Sohl-Dickstein, Diederik P. Kingma, Abhishek Kumar, Stefano Ermon, and Ben Poole. Score-based generative modeling through stochastic differential equations. In *The Ninth International Conference on Learning Representations, ICLR 2021*, 2021.
- [33] Yoshua Bengio, Li Yao, Guillaume Alain, and Pascal Vincent. Generalized denoising auto-encoders as generative models. *Advances in neural information processing systems*, 2013.
- [34] Zhisheng Xiao, Karsten Kreis, and Arash Vahdat. Tackling the generative learning trilemma with denoising diffusion gans. In *The Tenth International Conference on Learning Representations, ICLR, 2022*.
- [35] Diederik Kingma, Tim Salimans, Ben Poole, and Jonathan Ho. Variational diffusion models. *Advances in neural information processing systems*, 2021.
- [36] Alexander Quinn Nichol and Prafulla Dhariwal. Improved denoising diffusion probabilistic models. In *Proceedings of the 38th International Conference on Machine Learning, ICML, 2021*.
- [37] Prafulla Dhariwal and Alexander Quinn Nichol. Diffusion models beat gans on image synthesis. In *Advances in Neural Information Processing Systems*, 2021.
- [38] Geoffrey E Hinton. Training products of experts by minimizing contrastive divergence. *Neural computation*, 14(8):1771–1800, 2002.
- [39] Alex Krizhevsky and Geoffrey Hinton. Learning multiple layers of features from tiny images. 2009.
- [40] Jia Deng, Wei Dong, Richard Socher, Li-Jia Li, Kai Li, and Li Fei-Fei. Imagenet: A large-scale hierarchical image database. In *2009 IEEE Computer Society Conference on Computer Vision and Pattern Recognition, CVPR*, 2009.

- [41] Ziwei Liu, Ping Luo, Xiaogang Wang, and Xiaoou Tang. Deep learning face attributes in the wild. In *Proceedings of the 2015 International Conference on Computer Vision (ICCV)*, Santiago, Chile, 2015.
- [42] Martin Heusel, Hubert Ramsauer, Thomas Unterthiner, Bernhard Nessler, and Sepp Hochreiter. Gans trained by a two time-scale update rule converge to a local nash equilibrium. In Isabelle Guyon, Ulrike von Luxburg, Samy Bengio, Hanna M. Wallach, Rob Fergus, S. V. N. Vishwanathan, and Roman Garnett, editors, *Advances in Neural Information Processing Systems*, 2017.
- [43] Erik Nijkamp, Ruiqi Gao, Pavel Sountsov, Srinivas Vasudevan, Bo Pang, Song-Chun Zhu, and Ying Nian Wu. Learning energy-based model with flow-based backbone by neural transport mcmc. In *The Tenth International Conference on Learning Representations, ICLR, 2022*.
- [44] Zhisheng Xiao and Tian Han. Adaptive multi-stage density ratio estimation for learning latent space energy-based model. In *NeurIPS*, 2022.
- [45] Ruiqi Gao, Erik Nijkamp, Diederik P Kingma, Zhen Xu, Andrew M Dai, and Ying Nian Wu. Flow contrastive estimation of energy-based models. In *IEEE Conference on Computer Vision and Pattern Recognition, CVPR*, 2020.
- [46] Jianwen Xie, Zilong Zheng, and Ping Li. Learning energy-based model with variational auto-encoder as amortized sampler. In *AAAI Conference on Artificial Intelligence (AAAI)*, pages 10441–10451, 2021.
- [47] Jianwen Xie, Yang Lu, Ruiqi Gao, Song-Chun Zhu, and Ying Nian Wu. Cooperative training of descriptor and generator networks. *IEEE transactions on pattern analysis and machine intelligence*, 42(1):27–45, 2018.
- [48] Tian Han, Erik Nijkamp, Linqi Zhou, Bo Pang, Song-Chun Zhu, and Ying Nian Wu. Joint training of variational auto-encoder and latent energy-based model. In *IEEE Conference on Computer Vision and Pattern Recognition, CVPR*, 2020.
- [49] Yilun Du, Shuang Li, Joshua B. Tenenbaum, and Igor Mordatch. Improved contrastive divergence training of energy-based models. In *Proceedings of the 38th International Conference on Machine Learning, ICML*, 2021.
- [50] Jianwen Xie, Yaxuan Zhu, Jun Li, and Ping Li. A tale of two flows: Cooperative learning of langevin flow and normalizing flow toward energy-based model. In *The Tenth International Conference on Learning Representations, ICLR, 2022*.
- [51] Diederik P Kingma and Max Welling. Auto-encoding variational bayes. In *The Second International Conference on Learning Representations, ICLR*, 2014.
- [52] Tim Salimans, Andrej Karpathy, Xi Chen, and Diederik P Kingma. Pixelcnn++: Improving the pixelcnn with discretized logistic mixture likelihood and other modifications. In *The Fifth International Conference on Learning Representations, ICLR*, 2017.
- [53] Georg Ostrovski, Will Dabney, and Rémi Munos. Autoregressive quantile networks for generative modeling. In *Proceedings of the 35th International Conference on Machine Learning, ICML*, 2018.
- [54] Ricky TQ Chen, Jens Behrmann, David Duvenaud, and Jörn-Henrik Jacobsen. Residual flows for invertible generative modeling. In *Advances in Neural Information Processing Systems*, 2019.
- [55] Diederik P. Kingma and Prafulla Dhariwal. Glow: Generative flow with invertible 1x1 convolutions. In *Advances in Neural Information Processing Systems*, 2018.
- [56] Gaurav Parmar, Dacheng Li, Kwonjoon Lee, and Zhuowen Tu. Dual contradistinctive generative autoencoder. In *IEEE Conference on Computer Vision and Pattern Recognition, CVPR*, 2021.
- [57] Ishaan Gulrajani, Faruk Ahmed, Martin Arjovsky, Vincent Dumoulin, and Aaron Courville. Improved training of wasserstein gans. In *The Sixth International Conference on Learning Representations, ICLR*, 2017.
- [58] Takeru Miyato, Toshiki Kataoka, Masanori Koyama, and Yuichi Yoshida. Spectral normalization for generative adversarial networks. In *The Sixth International Conference on Learning Representations, ICLR*, 2018.

- [59] Andrew Brock, Jeff Donahue, and Karen Simonyan. Large scale GAN training for high fidelity natural image synthesis. In *The Seventh International Conference on Learning Representations, ICLR*, 2019.
- [60] Shengyu Zhao, Zhijian Liu, Ji Lin, Jun-Yan Zhu, and Song Han. Differentiable augmentation for data-efficient GAN training. In *Advances in Neural Information Processing Systems*, 2020.
- [61] Tero Karras, Miika Aittala, Janne Hellsten, Samuli Laine, Jaakko Lehtinen, and Timo Aila. Training generative adversarial networks with limited data. In *Advances in Neural Information Processing Systems*, 2020.
- [62] Yang Song and Stefano Ermon. Improved techniques for training score-based generative models. In *Advances in Neural Information Processing Systems*, 2020.
- [63] Eric Luhman and Troy Luhman. Knowledge distillation in iterative generative models for improved sampling speed. *arXiv preprint arXiv:2101.02388*, 2021.
- [64] Dongjun Kim, Seungjae Shin, Kyungwoo Song, Wanmo Kang, and Il-Chul Moon. Soft truncation: A universal training technique of score-based diffusion model for high precision score estimation. In *International Conference on Machine Learning, ICML*, 2021.
- [65] Tim Salimans, Ian J. Goodfellow, Wojciech Zaremba, Vicki Cheung, Alec Radford, and Xi Chen. Improved techniques for training gans. In Daniel D. Lee, Masashi Sugiyama, Ulrike von Luxburg, Isabelle Guyon, and Roman Garnett, editors, *Advances in Neural Information Processing Systems*, 2016.
- [66] Song Chun Zhu, Yingnian Wu, and David Mumford. Filters, random fields and maximum entropy (frame): Towards a unified theory for texture modeling. *International Journal of Computer Vision*, 27:107–126, 1998.
- [67] Yann LeCun, Sumit Chopra, Raia Hadsell, M Ranzato, and Fugie Huang. A tutorial on energy-based learning. *Predicting structured data*, 1(0), 2006.
- [68] Jiquan Ngiam, Zhenghao Chen, Pang Wei Koh, and Andrew Y. Ng. Learning deep energy models. In *Proceedings of the 28th international conference on machine learning, ICML*, 2011.
- [69] Geoffrey E. Hinton. A practical guide to training restricted boltzmann machines. In *Neural Networks: Tricks of the Trade - Second Edition*, pages 599–619. Springer, 2012.
- [70] Ruiqi Gao, Yang Lu, Junpei Zhou, Song-Chun Zhu, and Ying Nian Wu. Learning generative convnets via multi-grid modeling and sampling. In *IEEE Conference on Computer Vision and Pattern Recognition, CVPR*, pages 9155–9164, 2018.
- [71] Tong Che, Ruixiang Zhang, Jascha Sohl-Dickstein, Hugo Larochelle, Liam Paull, Yuan Cao, and Yoshua Bengio. Your gan is secretly an energy-based model and you should use discriminator driven latent sampling. *Advances in Neural Information Processing Systems*, 2020.
- [72] Taesup Kim and Yoshua Bengio. Deep directed generative models with energy-based probability estimation. *arXiv preprint arXiv:1606.03439*, 2016.
- [73] Rithesh Kumar, Sherjil Ozair, Anirudh Goyal, Aaron Courville, and Yoshua Bengio. Maximum entropy generators for energy-based models. *arXiv preprint arXiv:1901.08508*, 2019.
- [74] Tian Han, Erik Nijkamp, Xiaolin Fang, Mitch Hill, Song-Chun Zhu, and Ying Nian Wu. Divergence triangle for joint training of generator model, energy-based model, and inferential model. In *IEEE Conference on Computer Vision and Pattern Recognition, CVPR*, 2019.
- [75] Will Sussman Grathwohl, Jacob Jin Kelly, Milad Hashemi, Mohammad Norouzi, Kevin Swersky, and David Duvenaud. No MCMC for me: Amortized sampling for fast and stable training of energy-based models. In *The Ninth International Conference on Learning Representations, ICLR*, 2021.
- [76] Ian Goodfellow, Jean Pouget-Abadie, Mehdi Mirza, Bing Xu, David Warde-Farley, Sherjil Ozair, Aaron Courville, and Yoshua Bengio. Generative adversarial networks. *Communications of the ACM*, 63(11):139–144, 2020.
- [77] Olaf Ronneberger, Philipp Fischer, and Thomas Brox. U-net: Convolutional networks for biomedical image segmentation. In Nassir Navab, Joachim Hornegger, William M. Wells III, and Alejandro F. Frangi, editors, *Medical Image Computing and Computer-Assisted Intervention - MICCAI*, 2015.

- [78] Bradley Efron. Tweedie's formula and selection bias. *Journal of the American Statistical Association*, 106(496):1602–1614, 2011.
- [79] Herbert E Robbins. *An empirical Bayes approach to statistics*. Springer, 1992.

# Contents

<b>1</b>	<b>Introduction</b>	<b>1</b>
<b>2</b>	<b>Preliminaries on Energy-Based Models</b>	<b>2</b>
<b>3</b>	<b>Cooperative Diffusion Recovery Likelihood</b>	<b>2</b>
3.1	Diffusion recovery likelihood . . . . .	2
3.2	Amortizing MCMC sampling by initializer model . . . . .	3
3.3	Cooperative training . . . . .	4
3.4	Noise variance reduction . . . . .	4
3.5	Noise schedule and conditioning input . . . . .	4
3.6	Conditional sampling and classifier-free guidance of energy-based models . . . . .	5
3.7	Compositionality in energy-based model . . . . .	6
<b>4</b>	<b>Experiments</b>	<b>6</b>
4.1	Unconditional image generation . . . . .	7
4.2	Conditional synthesis with classifier-free guidance . . . . .	8
4.3	Compositionality . . . . .	8
4.4	Image inpainting . . . . .	9
<b>5</b>	<b>Related Work</b>	<b>9</b>
<b>6</b>	<b>Conclusion and Future Work</b>	<b>9</b>
<b>A</b>	<b>Training Details</b>	<b>16</b>
A.1	Network Structure . . . . .	16
A.2	Hyper-parameters . . . . .	16
<b>B</b>	<b>More Generation Results</b>	<b>17</b>
<b>C</b>	<b>Sampling time</b>	<b>17</b>
<b>D</b>	<b>Understand the role of initializer and EBMs</b>	<b>17</b>
<b>E</b>	<b>Ablation Study</b>	<b>18</b>
E.1	What are the contributions of each individual design component? . . . . .	18
E.2	Should the initializer be learned using the cooperative training algorithm or should it directly regress on the data? . . . . .	19
E.3	Whether adding more diffusion levels to the origin DRL schedule to cover the high-noise region works better than the new schedule used in CDRL? . . . . .	20
E.4	Can we further reduce the number of noise levels? . . . . .	20
E.5	What is the effect of using different number of Langevin steps? . . . . .	20

## A Training Details

### A.1 Network Structure

We adopt the EBM structure from [26], starting with a  $3 \times 3$  convolution layer with 128 channels (doubled to 256 in the CDRL(fat) setting). We use several downsample blocks for resolution adjustments, each containing multiple residual blocks. A  $2 \times 2$  average pooling layer is applied to all downsample blocks except the last. Spectral normalization is applied to all convolution layers for stability, while ReLU activation is applied to the final feature map. Spatial and channel dimensions are summed to obtain the energy output. EBM building block structures are shown in Table 3, and network architecture hyperparameters in Table 4.

For the initializer network, we follow [36]’s structure using a Unet [77] but with half the channels, reducing the initializer model size. For  $32 \times 32$  images, we have feature map resolutions at  $32 \times 32$ ,  $16 \times 16$ , and  $4 \times 4$ . For  $64 \times 64$  images, we add a  $64 \times 64$  resolution. We set all feature map channel numbers to 64 and apply attention to resolutions  $16 \times 16$  and  $8 \times 8$ . Our initializer directly outputs the noised image  $\tilde{y}_t$  at predicted level  $t$ , while [28] outputs total injected noise  $\epsilon$ .

For the class-conditioned generation task, we map class labels to one-hot vectors and use a fully-connected layer to map these vectors to class embedding vectors with the same dimensions as time embedding vectors. The class embedding is then added to the time embedding. We set the time embedding dimension to 512 for EBM and 256 for the initializer in the CDRL setting. In the CDRL(fat) setting, the time embedding dimension increases to 1024 for EBM, while the initializer’s dimension remains unchanged.

Table 3: Building block of the EBM.

(a) ResBlock	(b) Downsample Block	(c) Time Embedding
leakyReLU, $3 \times 3$ Conv2D	N ResBlocks	Sinusoidal Embedding
+ Dense(leakyReLU(temb))	Downsample $2 \times 2$	Dense, leakyReLU
leakyReLU, $3 \times 3$ Conv2D		Dense
+ Input		

Table 4: Structure hyper-parameter of EBM at different setting.

Model	M Downsample Blocks	N Resblocks Per Downsample Block	Number of Channels In Each Resolution
CDRL Image Size $32 \times 32$	4	8	(128, 256, 256, 256)
CDRL(fat) Image Size $32 \times 32$	4	8	(256, 512, 512, 512)
Compositionality Experiment	5	2	(128, 256, 256, 256, 256)
Inpainting Experiment	5	8	(128, 256, 256, 256, 256)

### A.2 Hyper-parameters

We set the learning rate of EBM to be  $\eta_\theta = 1e-4$  and the learning rate of initializer to be  $\eta_\phi = 1e-5$ . We use linear warm up for both EBM and initializer and let the initializer to start earlier than EBM. More specifically, given training iteration iter, we have:

$$\begin{aligned} \eta_\theta &= \min\left(1.0, \frac{\text{iter}}{10000}\right) \times 1e-4 \\ \eta_\phi &= \min\left(1.0, \frac{\text{iter} + 500}{10000}\right) \times 1e-5 \end{aligned} \tag{16}$$

We use Adam as optimizer for both EBM and initializer. We set the  $\beta_s = (0.9, 0.999)$  and weight decay equals to 0.0. We also applied exponential moving average which has decay equals to 0.9999

to both the EBM and initializer. We use 8 A100 GPU for training. The training process usually needs around 400k iterations, which takes up around 6 days.

Following [26], we use a re-parameterization trick for the calculating the energy term. We build our EBM on  $t = 0, 1, 2, 3, 4, 5$  and we assume the distribution of  $t = 6$  to be simple Normal distribution during sampling. Given  $\mathbf{y}_t$  under noise level  $t$ , suppose we denote the output of the EBM network as  $\hat{f}_\theta(\mathbf{y}_t, t)$ , then we let the true energy term to be  $f_\theta(\mathbf{y}_t, t) = \frac{\hat{f}_\theta(\mathbf{y}_t, t)}{s_t^2}$ , where  $s_t$  is the Langevin step size at noise level  $t$ , i.e. we parameterize the energy as the multiplication of EBM network output and a noise-level dependent coefficient and we set this coefficient to equal to the square of Langevin step size. We use 15 step Langevin updates at each noise level and we let the Langevin step size of noise level  $t$  to follow:

$$s_t^2 = 0.054 \times \bar{\sigma}_t \times \sigma_{t+1}^2 \quad (17)$$

$$(18)$$

where  $\sigma_{t+1}$  is the variance of the noise adding between noise level  $t$  and  $t + 1$  and  $\bar{\sigma}_t$  is the accumulative noise level at noise level  $t$ . During generation, we start from randomly sample  $x_6 \sim \mathcal{N}(0, \mathbf{I})$  and do denoising using both initializer and Langevin Dynamics following Algorithm 2. During image generation, after getting samples  $\mathbf{x}_0$  of the lowest noise level  $t = 0$ , we do one more denoising step without adding noise to further improve its quality. More specifically, we follow Tweedie’s formula [78, 79], which says that if we have  $\mathbf{x} \sim p_{data}(\mathbf{x})$  and noise version image  $\mathbf{x}'$  which has conditional distribution  $p(\mathbf{x}'|\mathbf{x}) = \mathcal{N}(\mathbf{x}, \sigma^2\mathbf{I})$ . The marginal distribution can be defined as  $p(\mathbf{x}') = \int p_{data}(\mathbf{x})p(\mathbf{x}'|\mathbf{x})d\mathbf{x}$ . Then we have

$$\mathbb{E}(\mathbf{x}|\mathbf{x}') = \mathbf{x}' + \sigma^2\nabla_{\mathbf{x}'} \log p(\mathbf{x}') \quad (19)$$

In our case, we have  $p(\mathbf{x}_t|\bar{\alpha}_t\mathbf{x}_0) = \mathcal{N}(\bar{\alpha}_t\mathbf{x}_0, \bar{\sigma}_t^2\mathbf{I})$  and we use EBM to model the marginal distribution of  $\mathbf{x}_t$  as  $p_{\theta,t}(\mathbf{x}_t)$ , thus:

$$\begin{aligned} \mathbb{E}(\bar{\alpha}_t\mathbf{x}_0|\mathbf{x}_t) &= \mathbf{x}_t + \bar{\sigma}_t^2\nabla_{\mathbf{x}_t} \log p_{\theta,t}(\mathbf{x}_t) \\ \mathbb{E}(\mathbf{x}_0|\mathbf{x}_t) &= \frac{\mathbf{x}_t + \bar{\sigma}_t^2\nabla_{\mathbf{x}_t} \log p_{\theta,t}(\mathbf{x}_t)}{\bar{\alpha}_t} \end{aligned} \quad (20)$$

Suppose the samples we get at  $t = 0$  is  $x_0$ . This samples actually contains a small magnitude of noise corresponding to  $\bar{\alpha}_0$ , thus, we may use Equation 20 to further denoise it. In practice, we find that enlarging the denoising step by multiplying gradient term  $\nabla_{\mathbf{x}_t} \log p_{\theta,t}(\mathbf{x}_t)$  by a coefficient larger than 1.0 gives us better results. We set this coefficient to be 2.0 in our experiments.

## B More Generation Results

In this section we show more generation results. Figure 7 shows more compositionality results with different guidance weight on CelebA  $64 \times 64$  dataset. Here,  $w = 0.0$  equals to the original setting in Equation 14 in the main paper without guidance. In Figure 8, 9, 10, 11 and 12 provide more results for conditional generation on ImageNet32 ( $32 \times 32$ ) with different guidance weight. Figure 8 gives random samples while each figure in Figure 9, 10, 11 and 12 contains samples from a certain class under different guidance weight  $w$ .

## C Sampling time

In this section, we measure the sampling time of CDRL and compare it with the following models: 1) Short-run EBM [2] with the same EBM structure as DRL; 2) VAEBM [6], which composes a VAE with an EBM and achieves strong generation performance; 3) The original DRL [26] model with 30 step MCMC steps at each noise level. We run the sampling process of each model individually on a single A100 GPU to generate a batch of 100 samples on the Cifar10 dataset. Our CDRL model uses less computing time for generating the same amount of images.

## D Understand the role of initializer and EBM

To further understand the roles of our initializer and EBM in image generation, we conduct two additional experiments using a pretrained CDRL model on the ImageNet Dataset ( $32 \times 32$ ). We

Table 5: Comparison of different EBMs in terms of sampling time and number of MCMC steps. The sampling time are measured in second.

Method	Number of MCMC steps	Sampling Time
Short-run EBM[2]	100	12.7
VAEBM [6]	16	21.3
DRL [26]	6(noise level) $\times$ 30 (steps at each level)	23.9
CDRL (Ours)	6(noise level) $\times$ 15 (steps at each level)	12.2

evaluate two generation options: (a) images generated using only the initializer’s proposal, without the EBM’s Langevin Dynamics at each noise level, and (b) images generated with the full CDRL model, which includes the initializer’s proposal and 15-step Langevin updates at each time interval. As shown in Figure 6a and 6b, the initializer captures the object’s rough outline, while the Langevin updates on EBM fill in meaningful details. Furthermore, in Figure 6c, we display samples generated by fixing the initial noise image and sample noise of each initializer proposal step. The results reveal that images generated with the same initialization noises share basic elements while differing in details, highlighting the impact of both the initializer and Langevin sampling. The initializer provides a starting point, and the Langevin sampling process adds details.

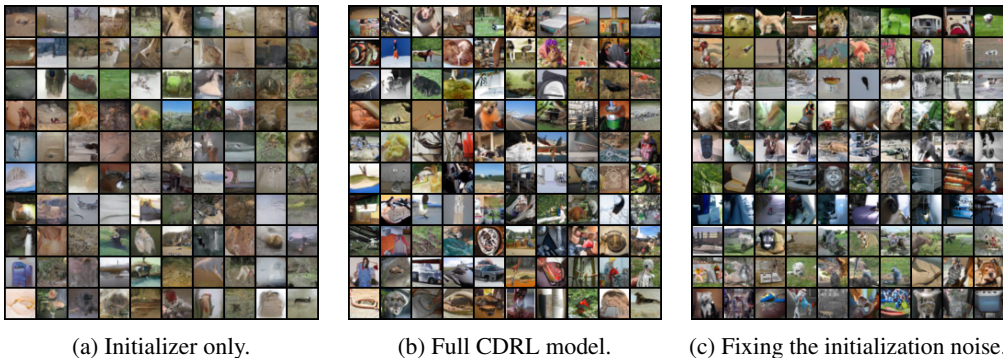


Figure 6: Illustration of the effect of initializer and EBM in the image generation process with a CDRL model pretrained on ImageNet Dataset ( $32 \times 32$ ). (a) Samples generated using only the proposal of the initializer; (b) Samples generated by the full CDRL model; (c) Samples generated by fixing the initial noise image and the sample noise of each initialization proposal step. Each row of images shared the same initial noise image and the sample noise of each initialization proposal step, but differed in the noises of Langevin sampling process at each noise level.

## E Ablation Study

In this section, we carry out ablation studies to justify the choice of each component of our CDRL model. We use several experiments to answer the questions listed below.

### E.1 What are the contributions of each individual design component?

In our main paper, we have described the three main techniques that contribute most to our CDRL model. They are the new noise schedule design, cooperative training algorithm and noise variance reduction. Here, we demonstrate the effect of each of the three techniques by comparing our CDRL with the following models (1) The original DRL model used in [26]; (2) Model trained without cooperatively training framework: This corresponds to the original recovery-likelihood EBM using the same noise schedule and conditioning input as CDRL; (3) CDRL without noise reduction; (4) While CDRL use initializer to directly output  $\hat{y}_t$ , here similar to [34], we use the initializer to output the prediction of clean image  $\hat{x}_0$  and then transformed it to  $\hat{y}_t$ . (5) Similarly, we can also use initializer to directly output the prediction of total added noise  $\hat{e}$  similar to [28] and then transformed it to  $\hat{y}_t$ .

Table 6: Ablation study on CIFAR-10 dataset.

Models	FID ↓
DRL [26]	9.58
No cooperative training	6.47
No noise reduction	5.51
Initializer predicts $\hat{\mathbf{x}}_0$	5.17
Initializer predicts $\hat{\epsilon}$	4.95
CDRL	4.31

We let all the models to share the same network structure and training setting on CIFAR-10 dataset and differ only in the way mentioned above. Shown in Table 6, our full model works the best among these settings, which justifies our design choice.

## E.2 Should the initializer be learned using the cooperative training algorithm or should it directly regress on the data?

Shown in equation 8 in the main paper, in our cooperative training algorithm, the initializer learns from the revised sample  $\tilde{\mathbf{y}}_t$  at each step. A natural question to be asked here is whether we should instead regress it directly on data  $\mathbf{y}_t$ . To answer this, we try the option that the initializer directly learns from  $\mathbf{y}_t$  at each step. We denote this option as CDRL(data) to distinguish it from the original CDRL model. The results shown in Table 7 suggest that CDRL works better than CDRL(data), which supports our choice of the cooperative training algorithm.

To understand this, we may first dive into a deeper understanding of the learning behavior of the cooperative learning algorithm. We follow the analysis framework of [2, 50]. Let  $K_\theta(\mathbf{y}_t|\mathbf{y}'_t, \mathbf{x}_{t+1})$  be the transition kernel of the  $T$ -step Langevin sampling that refines the initial output  $\mathbf{y}'_t$  to the refined output  $\mathbf{y}_t$ . Let  $(K_\theta q_\phi)(\mathbf{y}_t|\mathbf{x}_{t+1}) = \int K_\theta(\mathbf{y}_t|\mathbf{y}'_t, \mathbf{x}_{t+1})q_\phi(\mathbf{y}'_t|\mathbf{x}_{t+1})d\mathbf{y}'_t$  be the conditional distribution of  $\mathbf{y}_t$ , which is obtained by  $T$  steps of Langevin sampling starting from the output of the initializer  $q_\phi(\mathbf{y}_t|\mathbf{x}_{t+1})$ . Let  $\pi(\mathbf{y}_t|\mathbf{x}_{t+1})$  be the true conditional distribution for denoising  $\mathbf{x}_{t+1}$  to retrieve  $\mathbf{y}_t$ . The maximum recovery likelihood for the EBM in equation 4 in the main paper is equivalent to minimizing the KL divergence  $KL(\pi(\mathbf{x}_t|\mathbf{y}_{t+1})||p_\theta(\mathbf{x}_t|\mathbf{y}_{t+1}))$ . Let us use  $j$  to index the learning iteration for model parameters. Given the current initializer model  $q_\phi(\mathbf{y}_t|\mathbf{x}_{t+1})$ , the EBM updates its parameters  $\theta$  by minimizing

$$\theta_{j+1} = \arg \min_{\theta} KL(\pi(\mathbf{y}_t|\mathbf{x}_{t+1})||p_\theta(\mathbf{y}_t|\mathbf{x}_{t+1})) - KL((K_{\theta_j} q_\phi)(\mathbf{y}_t|\mathbf{x}_{t+1})||p_\theta(\mathbf{y}_t|\mathbf{x}_{t+1})) \quad (21)$$

which is modified contrastive divergence. It is worth noting that, in the original contrastive divergence, the above  $(K_{\theta_j} q_\phi)(\mathbf{y}_t|\mathbf{x}_{t+1})$  is replaced by  $(K_{\theta_j} \pi)(\mathbf{y}_t|\mathbf{x}_{t+1})$ . That is, the MCMC chains are initialized by the true data. The learning shifts  $p_\theta(\mathbf{y}_t|\mathbf{x}_{t+1})$  toward the true distribution  $\pi(\mathbf{y}_t|\mathbf{x}_{t+1})$ .

On the other hand, given the current EBM, the initializer model learns from the output distribution of the EBM’s MCMC. (That is, we train the initializer with  $\tilde{\mathbf{y}}$  in equation 8 of the main paper.) The update of the parameters of the initializer at learning iteration  $j + 1$  approximately follows the gradient of

$$\phi_{j+1} = \arg \min_{\phi} KL(K_\theta q_{\phi_j}(\mathbf{y}_t|\mathbf{x}_{t+1})||q_\phi(\mathbf{y}_t|\mathbf{x}_{t+1})) \quad (22)$$

The initializer  $q_\phi(\mathbf{y}_t|\mathbf{x}_{t+1})$  learns to be the stationary distribution of the MCMC transition  $K_\theta(\mathbf{x}_t|\mathbf{y}_{t+1})$  by shifting its mapping to the low energy regions of  $p_\theta(\mathbf{x}_t|\mathbf{y}_{t+1})$ . In a limit, the initializer  $q_\phi(\mathbf{y}_t|\mathbf{x}_{t+1})$  minimizes  $KL(K_\theta q_{\phi_j}(\mathbf{y}_t|\mathbf{x}_{t+1})||q_\phi(\mathbf{y}_t|\mathbf{x}_{t+1}))$  and gets close to the EBM  $p_\theta(\mathbf{x}_t|\mathbf{y}_{t+1})$ . The whole learning algorithm is a chasing game. That is, the initializer model  $q_\phi(\mathbf{y}_t|\mathbf{x}_{t+1})$  chases the EBM  $p_\theta(\mathbf{y}_t|\mathbf{x}_{t+1})$  toward the true distribution  $\pi(\mathbf{y}_t|\mathbf{x}_{t+1})$ .

Table 7: Comparison between the model whose initializer learns from the samples given by EBM and the one whose initializer learns directly from the data. Scores are reported on Cifar-10 dataset.

Model	FID ↓
CDRL(data)	5.95
CDRL	4.31

Then we can begin the discussion of the benefits of the cooperative learning. Comparing with training the initializer directly with observed  $\mathbf{y}$ , the proposed training with  $\tilde{\mathbf{y}}$  has the following benefits.

Firstly, in our algorithm, Equation 22 above shows that the MCMC of the EBM drives the evolution of the initializer that seeks to amortize the MCMC. At each learning iteration, in order to provide good initial examples for the current EBM’s MCMC, the initializer needs to be close enough to the EBM. Therefore, at each learning algorithm, training the initializer with the MCMC outputs  $\tilde{\mathbf{y}}$  is a good strategy to maintain a proper distance between EBM and initializer model. If the initializer directly learns from the true distribution, even though it can move toward the true distribution quickly, it might not provide a good starting point for the MCMC. A good initializer should be helpful for finding the modes of the EBM. Let us imagine a situation in which the initializer model has shifted toward the true distribution by firstly learning directly with  $\mathbf{y}$ , but the EBM is still far from that. Due to a large divergence between EBM and initializer, the initializer is not helpful for EBM to draw fair samples, especially with a finite-step Langevin dynamics. A far-away initializer might lead to unstable training of the EBM.

Secondly, to consider a more generic case, in which we model our initializer via a non-Gaussian generator  $\mathbf{y}_t = g_\phi(\mathbf{x}_{t+1}, \mathbf{z}, t)$ ,  $\mathbf{z} \sim \mathcal{N}(0, \mathbf{I})$ . The randomness comes from the latent vector  $\mathbf{z}$ . In this case  $q_\phi(\mathbf{y}_t|\mathbf{x}_{t+1}) = \int p(\mathbf{y}_t|\mathbf{x}_{t+1}, \mathbf{z})p(\mathbf{z})d\mathbf{z}$  is analytically intractable. Learning  $q_\phi(\mathbf{y}_t|\mathbf{x}_{t+1})$  directly from  $\mathbf{y}$  independently requires MCMC inference for the posterior distribution  $q_\phi(\mathbf{z}|\mathbf{x}_{t+1}, \mathbf{y}_t)$ . However, the cooperative learning can get around the difficulty of inference of the latent variables  $\mathbf{z}$ . That is, at each learning iteration, we generate examples  $\hat{\mathbf{y}}$  from  $q_\phi(\mathbf{y}_t|\mathbf{x}_{t+1})$  by first sampling  $\hat{\mathbf{z}} \sim p(\mathbf{z})$  and then mapping it to  $\hat{\mathbf{y}}_t = g_\phi(\mathbf{x}_{t+1}, \hat{\mathbf{z}}, t)$ . The  $\hat{\mathbf{y}}$  is used to initialize the EBM’s MCMC that produces  $\tilde{\mathbf{y}}$ . The learning equation of  $\phi$  is  $\frac{1}{n} \sum_{i=1}^n -\frac{1}{2\sigma_t^2} \|\mathbf{y}_{t,i} - g_\phi(\mathbf{x}_{t+1,i}, \hat{\mathbf{z}}, t)\|^2$ , where the latent variables  $\hat{\mathbf{z}}$  is used. That is, we shift the mapping from  $\hat{\mathbf{z}} \rightarrow \hat{\mathbf{y}}$  to  $\hat{\mathbf{z}} \rightarrow \tilde{\mathbf{y}}$  for accumulate the MCMC transition. Even though in our paper, we currently use a Gaussian initializer, if we use a non-Gaussian initializer in the future, the current cooperative learning (i.e., training  $q_\phi$  with  $\tilde{\mathbf{y}}$ ) can be much more beneficial and feasible.

Table 8: Comparison between our CDRL model with the model using DRL noise level schedule but adding 2 more noise levels to the high noise region. Scores are reported on Cifar-10 dataset.

Model	FID ↓
CDRL(DRL-T8)	4.94
CDRL	4.31

### E.3 Whether adding more diffusion levels to the origin DRL schedule to cover the high-noise region works better than the new schedule used in CDRL?

In section 3.5, we introduce the new noise schedule we used for CDRL. Comparing with the one used in the original DRL[26] paper, the noise schedule used in CDRL puts more attention on the high-noise area where  $\bar{\alpha}$  is close to 0. We carry out a comparison that trains the CDRL model using the original DRL schedule but with 2 more extra noise levels in the high-noise region. We refer to this setting as CDRL(DRL-T8). As shown in Table 8, CDRL(DRL-T8) performs slightly worse than CDRL. Also, in terms of sampling time, CDRL(DRL-T8) required 30% more steps during sampling. That is, increasing the number of noise levels might not necessarily improve the performance, but it must increase the computational cost. Our new schedule is very important because it keeps the algorithm efficient.

### E.4 Can we further reduce the number of noise levels?

We test whether the noise level can be further reduced. The results in Table 9a show that further reducing noise level to 4 can make model more unstable even if we increase the number of the Langevin sample steps  $L$ . On the other hand reducing  $T$  to 5 gives reasonable but slightly worse results.

### E.5 What is the effect of using different number of Langevin steps?

In Table 9b, we show the effect of changing the number of Langevin steps  $L$ . The results show that, on one hand, decreasing  $L$  to 10 gives us comparable but slightly worse results. On the other hand, increasing  $L$  to 30 doesn’t give better results. This agrees with the observations by DRL[26]. The observation of changing  $L$  implies that simply increasing the number of Langevin steps doesn’t bring

significant increase in the sample quality, which verifies the effectiveness of the initializer in our model.

Table 9: CDRL with different number of noise levels  $T$  and number of Langevin steps  $L$ . Scores are reported on Cifar-10 dataset.

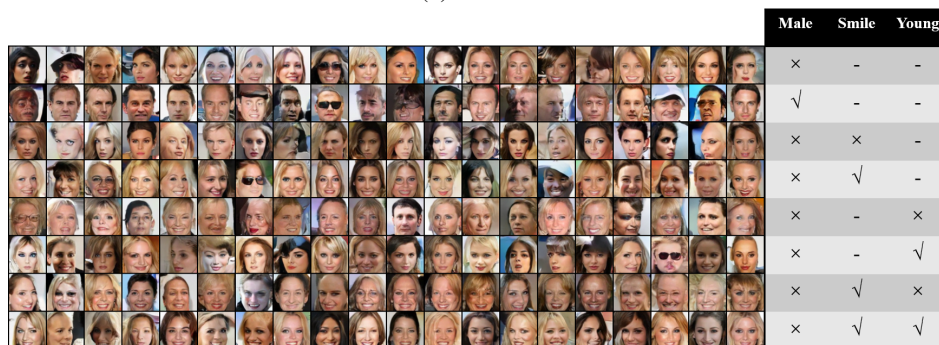
(a) Results for reducing $T$		(b) Results for changing $L$	
Model	FID ↓	Model	FID ↓
T=4 (L=15,20,30)	- (not converge)	T=6 (L=10)	4.50
T=5 (L=15)	5.08	T=6 (L=15)	4.31
T=6 (L=15)	4.31	T=6 (L=30)	5.08



(a)  $w = 0.0$



(b)  $w = 0.5$



(c)  $w = 1.0$

Figure 7: Attribute compositional samples on CelebA ( $64 \times 64$ ). Here we use guided weight  $w = 0.0, 0.5, 1.0$ . We let images at different guidance share the same random noise. Results can also be compared with Figure 4 which use  $w = 3.0$

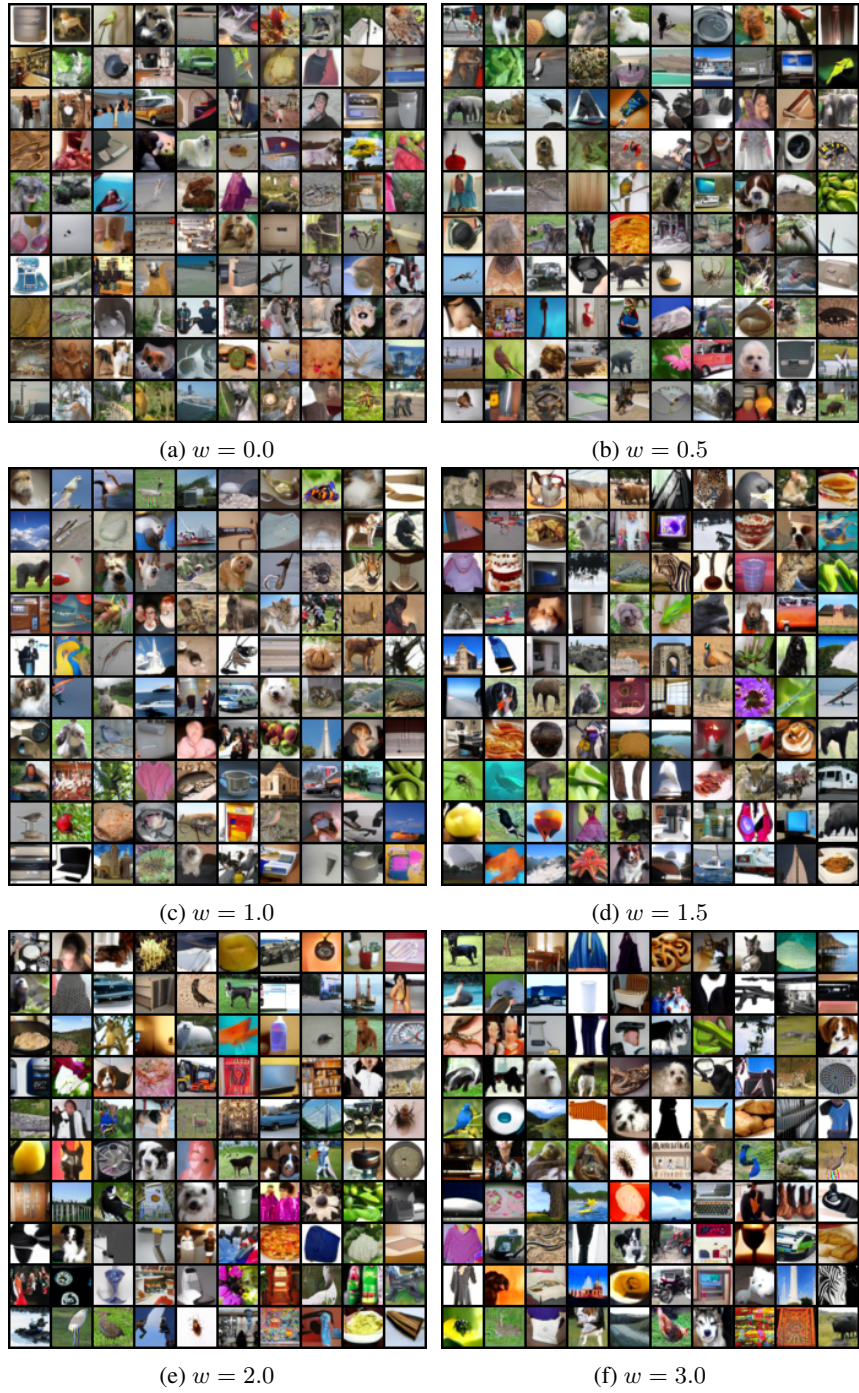


Figure 8: Conditional generated examples with different classifier free guidance weight on ImageNet32 ( $32 \times 32$ ). Samples are generated with randomly chosen class label.



Figure 9: Conditional generated examples with different classifier free guidance weight on ImageNet32 ( $32 \times 32$ ) with class label Tench.

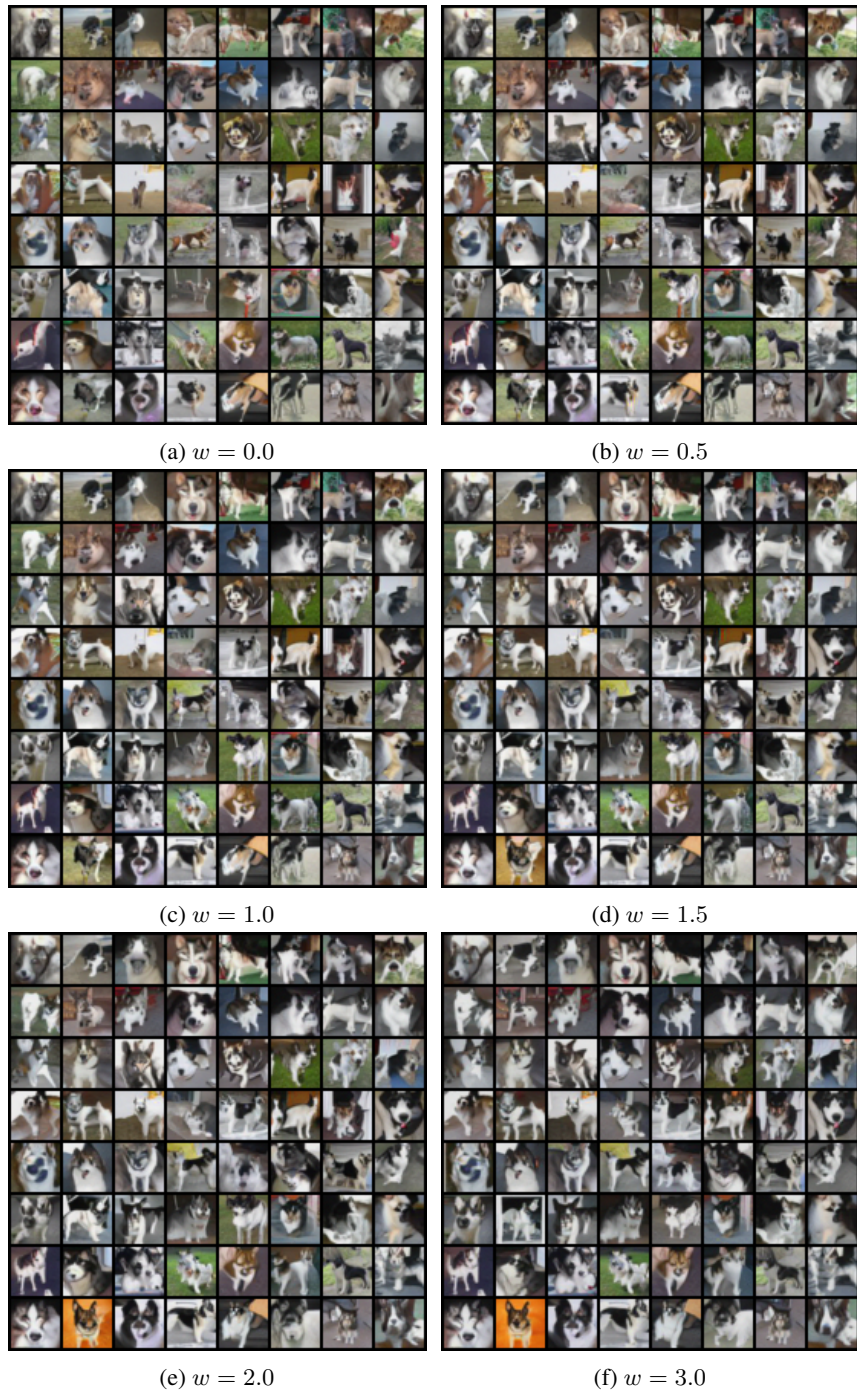


Figure 10: Conditional generated examples with different classifier free guidance weight on ImageNet32 (32 × 32) with class label Siberian Husky.



Figure 11: Conditional generated examples with different classifier free guidance weight on ImageNet32 ( $32 \times 32$ ) with class label Tow Truck.

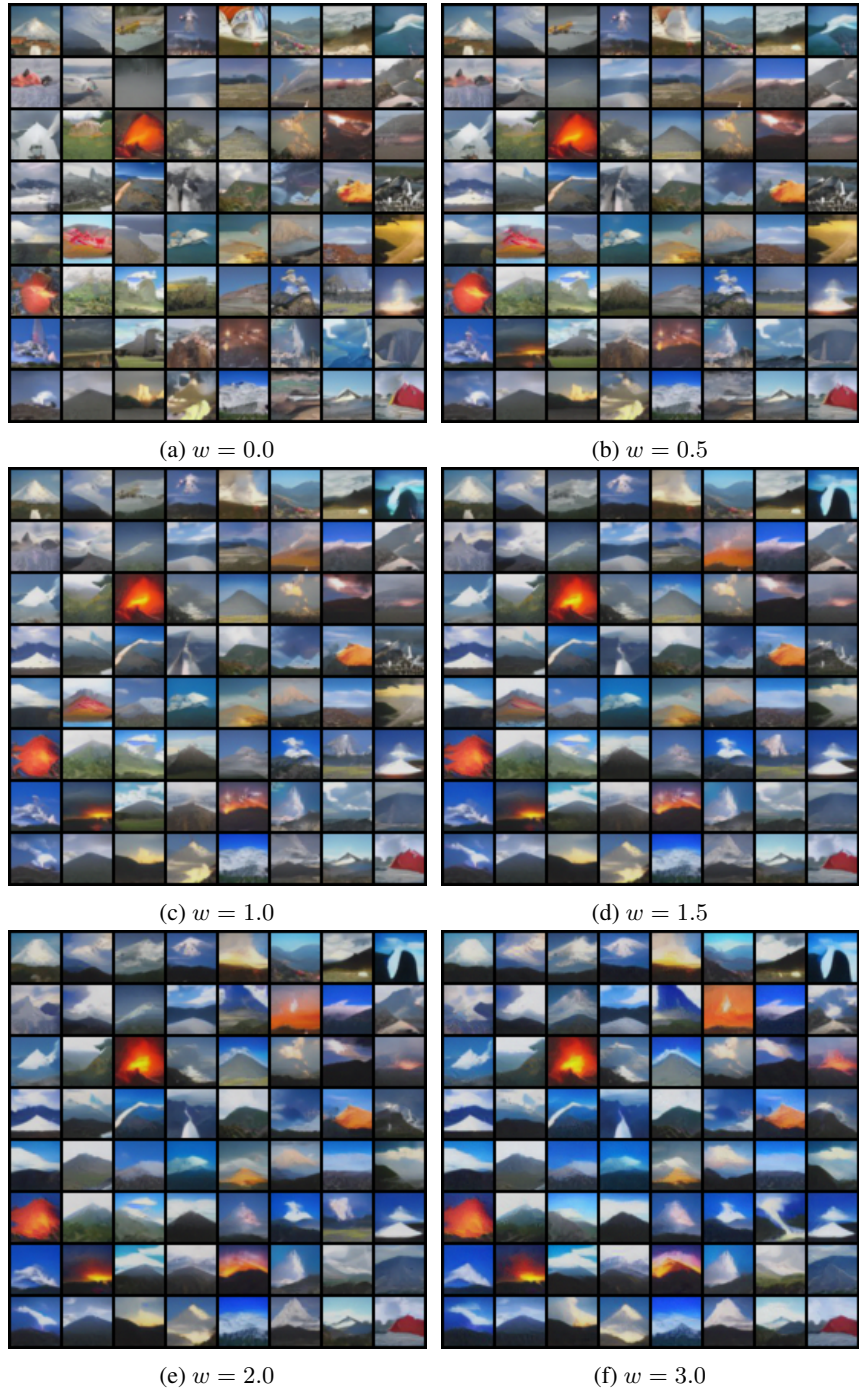


Figure 12: Conditional generated examples with different classifier free guidance weight on ImageNet32 (32 x 32) with class label Volcano.